

2.0 OSIRIS HIB-DRIVEN POWER PLANT

2.1 SUMMARY OF OSIRIS PLANT PARAMETERS

Osiris is a 1000 MWe, HIB-driven power plant design. The Osiris Chamber is of the thick liquid-wall family, a descendent of HYLIFE,² HIBALL,³ Pulse*Star,⁴ and HYLIFE-II.⁵ The Osiris chamber design features a porous carbon fabric blanket that is filled with the molten salt Flibe (2LiF-BeF₂). A key feature of Osiris is the use of low activation ceramics in a configuration in which brittleness and leak-tightness are not issues. A thin layer of liquid Flibe coats the carbon fabric first wall to protect it from x-ray and debris damage. Part of this protective layer is vaporized with each pulse. The vaporized Flibe condenses in a spray at the bottom of the chamber. Flibe circulates through the blanket and serves as the primary coolant and tritium breeding material. The blanket support structures and vacuum vessel are made of low activation carbon/carbon composites. Liquid lead is used in the intermediate loop to transfer heat to a steam generator and a double reheat steam power cycle.

The heavy ion driver uses singly-charged xenon ions. The design approach is conservative in that it does not use beam combination, separation, or recirculation. The design maximizes component standardization. It uses a propagation mode in the accelerator with constant beam radius, high-performance Nb₃Sn quadrupoles with constant strength and length, and a single quadrupole array configuration. There are only two inductor cell designs, one each for low and high energy. Illumination of the target is double-sided with six beams from each side.

The key plant operating parameters are listed in Table 2.1.

2.2 OSIRIS CHAMBER DESIGN

The Osiris chamber is shown in Fig. 2.1, and the key chamber design parameters are given in Table 2.2. The first wall and blanket are made of a flexible, woven carbon fabric that is stitched together much like a tent. To minimize stress on the fabric from the hydrostatic and pressure head of the Flibe, the fabric blanket is constructed like an air mattress, as shown in Fig. 2.2. Flibe enters the top of the chamber at 500°C and flows down the 5-cm-thick flow channel behind the first wall at a maximum velocity of 5 m/s. A small fraction of the Flibe flows through the porous fabric first wall to provide a protective liquid layer. The fabric weave is adjusted to control the flow rate through the first wall. The high flow rate in the first wall channel limits the temperature rise of the Flibe near the first wall. Therefore, the Flibe that weeps through the fabric to coat the

Table 2.1. Osiris Power Plant Operating Parameters

| | |
|---------------------------------|------|
| Driver Energy (MJ) | 5.0 |
| Target Gain | 86.5 |
| Target Yield (MJ) | 432 |
| Rep rate (Hz) | 4.6 |
| Fusion Power (MW) | 1987 |
| Energy Multiplication | 1.26 |
| Total Thermal Power (MW) | 2504 |
| Power Conversion Efficiency (%) | 45 |
| Gross Electrical Power (MWe) | 1127 |
| Driver Efficiency (%) | 28 |
| Driver Power (MWe) | 82 |
| Auxiliary Power (MWe) | 45 |
| Net Electric Power (MWe) | 1000 |
| Tritium Breeding Ratio | 1.24 |

first wall is always near the cold-leg temperature. This helps maintain the low pressure conditions needed for beam propagation.

After flowing down the backside of the first wall, the Flibe coolant turns and flows upward, absorbing the neutron heat. It exits the blanket at the top and cascades down the outside with considerable turbulence, releasing some of the bred tritium to the vacuum system.

The target yield per pulse is 432 MJ. About 30% of this energy is in x-rays and debris and results in the vaporization of ~4.2 kg of Flibe from the protective layer. The impulse due to the blowoff was calculated to be 90 Pa-s at $R = 3.5$ m. Because the Flibe and carbon have comparable impedances, the kinetic energy from this blowoff will be distributed throughout the blanket. The kinetic energy is a negligible 0.05 J/m². Volumetric heating from the neutrons near the first wall is 5 J/cm³, giving a temperature rise per pulse of only one degree.

With the tent-like geometry of the chamber, the blowoff vapor is preferentially directed toward the spray and pool at the bottom of the chamber. The 46 m/s spray is supplied with Flibe at the cold-leg temperature of 500°C to enhance condensation. The vaporized Flibe is "cryopumped" by the Flibe spray and pool down to the required 5×10^{18} atoms/m³ in less than 60 ms, well below the 220 ms interpulse time. Because the vapor is condensed in the spray and pool, there is very little heat transfer through the first wall. Flibe from the pool and the Flibe from the neutron blanket drain from the bottom of the chamber with an average outlet temperature of 650°C.

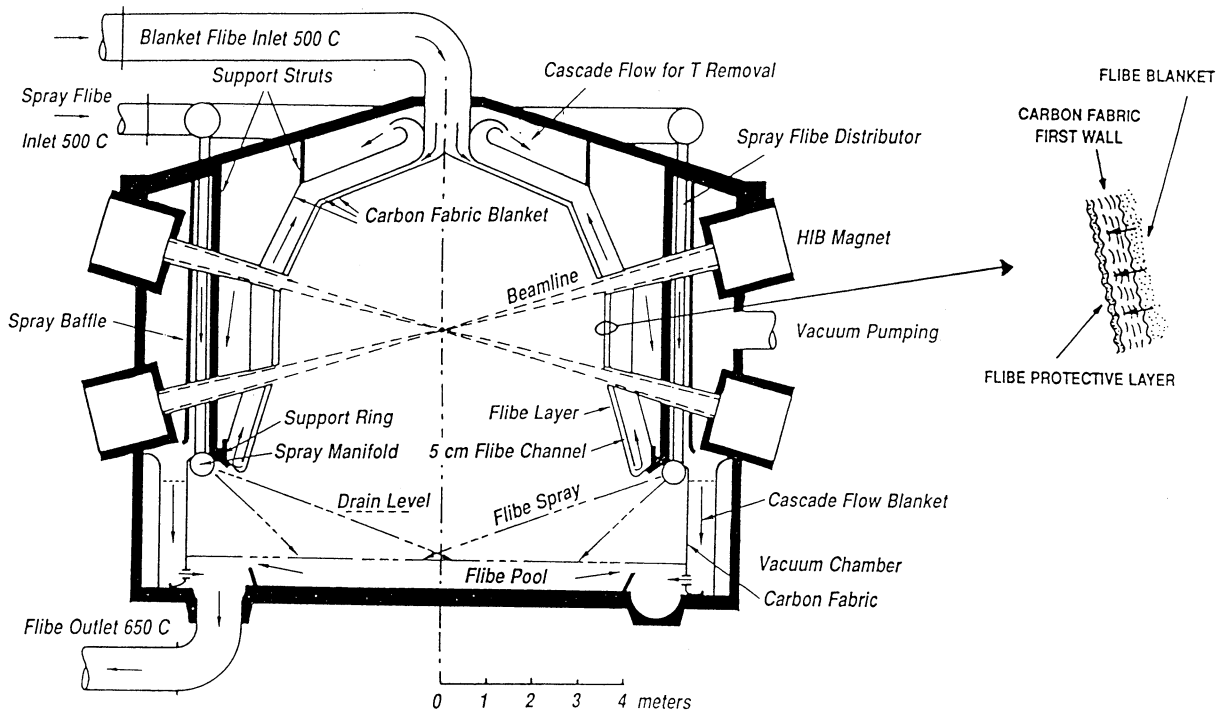


Fig. 2.1. Osiris chamber design.

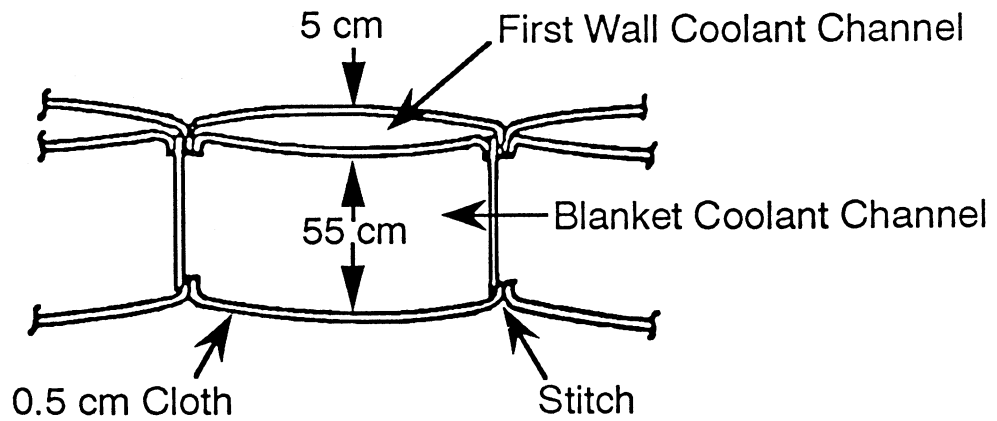


Fig. 2.2. Cross section of the carbon fabric blanket.

Table 2.2. Osiris Chamber Design Parameters

| | |
|----------------------------------------|---------|
| First Wall Radius at Midplane (m) | 3.5 |
| Flibe Vaporized per Shot (kg) | 4.2 |
| Peak Pressure on First Wall (GPa) | 37 |
| Impulse on First Wall (Pa-s) | 90 |
| Blanket Thickness (m) | 0.7 |
| Total Thermal Power (MW) | 2504 |
| Surface Power (MW) | 596 |
| Blanket Power (MW) | 1908 |
| Flibe Inlet Temperature (°C) | 500 |
| Flibe Outlet Temperature (°C) | 650 |
| Spray Flow Rate (kg/s) | 2265 |
| Blanket Flow Rate (kg/s) | 4598 |
| Max. First Wall Channel Velocity (m/s) | 5 |
| Flibe Upflow Average Velocity (m/s) | 0.2 |
| Spray Velocity (m/s) | 46 |
| Spray Manifold Pressure (MPa) | 2.1 |
| Spray Ideal Pumping Power (MW) | 3 |
| Total Flibe Mass in Chamber (kg) | 456,000 |
| Total Supported Mass (kg) | 274,000 |
| Main Support Hanger Diameter (m) | 0.1 |
| Number of Hangers | 24 |
| Hanger Tensile Stress (MPa) | 14 |
| Total Flibe Inventory (kg) | 940,000 |

The Osiris blanket has excellent neutronic performance in terms of tritium breeding and energy multiplication. The reference design has a 60-cm-thick main blanket plus 10 cm cascade flow along the outside of the blanket. This gives a tritium breeding ratio of 1.24 with 1.10 coming from ${}^6\text{Li}$. The energy multiplication factor is 1.26, which boosts the 1987 MW of fusion power to 2504 MW of total thermal power. The displacement damage rate in the carbon fabric first wall is about 42 dpa/full power year (fpy), and the helium production rate is about 1100 appm/fpy. While the damage limits for the carbon fabric are uncertain, we estimated a first wall life of 1.8 fpy. The maintenance scheme for the Osiris first wall, however, is very simple and should

not significantly increase the down-time of the power plant. The entire fabric assembly, drained of Flibe, is lifted out the top and replaced with a new assembly.

The vacuum vessel for Osiris is constructed of a low-activation carbon/carbon composite and is at a radius of ~6.5 m. The Flibe blanket effectively reduces the radiation damage and helium production rates to the composite vacuum vessel wall to 0.2 dpa/fpy and 10 appm/fpy, respectively. This component is, therefore, expected to last the full 30 year life of the plant.

2.3 OSIRIS POWER CONVERSION AND PLANT FACILITIES

2.3.1 Heat Transport System

The primary coolant for Osiris is liquid Flibe. Flibe enters the chamber at 500°C and exits at 650°C. The primary loop consists of two coolant circuits including one intermediate heat exchanger (IHX) in each circuit. Two circuits are used to keep the size of the IHXs from getting too large.

An intermediate coolant loop is used to isolate the primary coolant, which will contain radioactive elements, from the steam cycle. The intermediate loop consists of two circuits including one steam generator in each circuit. Liquid lead, operating between 400 and 600°C, is the intermediate coolant. It offers a safety advantage over sodium, which was considered as a possible alternative. While modest technology extrapolation is needed for the steam generators, their size appears to be reasonable.

To achieve a high efficiency power conversion, a high pressure/high temperature steam cycle is used. The steam pressure and temperature conditions chosen are consistent with the intermediate coolant temperature. These conditions also represent the state-of-the-art steam conditions used for fossil-fired steam power plants. A double-reheat steam cycle is used with the peak steam pressure and temperature of 24.2 MPa (3500 psig) and 538°C (1000°F), respectively. These conditions provide a power conversion efficiency of 45%.

There are two steam generators, and each is sized to handle half of the plant thermal output. Thus the thermal rating of each steam generator is 1250 MWt. To accommodate the double reheat feature of the power cycle, each steam generator is made up of three separate vessels: superheater, first reheater, and second reheater. These steam generator vessels are supplied with liquid lead from the IHXs.

The reactor plant is provided with a turbine-generator capable of generating 1127 MWe gross electrical power. The turbine-generator is a state-of-the-art design consisting of one high-pressure section, one intermediate-pressure section, and two low-pressure sections arranged in a cross-compound configuration.

2.3.2 Reactor Building

The reactor building provides housing for the reactor and shielding of the public from fusion neutrons. In addition, the building also accommodates remote maintenance of the reactor. The reactor building size is dictated by the maintenance handling requirements for the vacuum vessel cover and reactor internals. The conceptual arrangement of the building is shown in Figs. 2.3 and 2.4. The reactor is located at the center of the reactor hall. The IHXs are located in a separate hall so that the area can be accessed for limited periods during normal power operation; the reactor hall is provided with requisite shielding for this purpose. The nearest shielding wall is 10 m from the center of the chamber, and the shield thickness is 3.2 m.

Another feature of the reactor building is that there is no direct piping penetration between the reactor and IHX halls. The primary coolant piping is routed via an underground piping tunnel; there is no direct neutron path from the reactor hall to the IHX hall. The shield wall of the IHX hall is 1 m thick to allow unlimited access to the steam generator building.

2.4 HEAVY-ION DRIVER DESIGN

2.4.1 Summary of Results

The base 5-MJ heavy-ion induction driver design uses conservative design assumptions and has an efficiency of 28% and a direct cost of only \$120/J. Combining the driver efficiency with an estimated target gain of 86.5 gives a recirculating power fraction for a 1000 MWe plant of only ~7%. We created a high-performance, low-cost design by

- using an original design for compact arrays of high-performance, Nb₃Sn quadrupoles that leads to small sizes and costs for the inductor cells as well as for the focusing arrays, and
- conducting a parametric search over a wide range of possible driver parameters to choose parameters that give an attractive design.

We use minimal extrapolation from existing accelerator technology and physics to create highly credible driver performance. We do not use any bends in the accelerator, beam combination, or beam separation. Although driver designs with bends, such as recirculating induction accelerators, offer the potential for cost savings by bending the beams in a circle and reducing the number of required driver elements, present performance uncertainties are large for high-current circular accelerators. Linear driver costs and projected target gains could be improved by combining beams early in the driver and separating them before final focusing; again we avoid performance uncertainties by not using beam combination or separation.

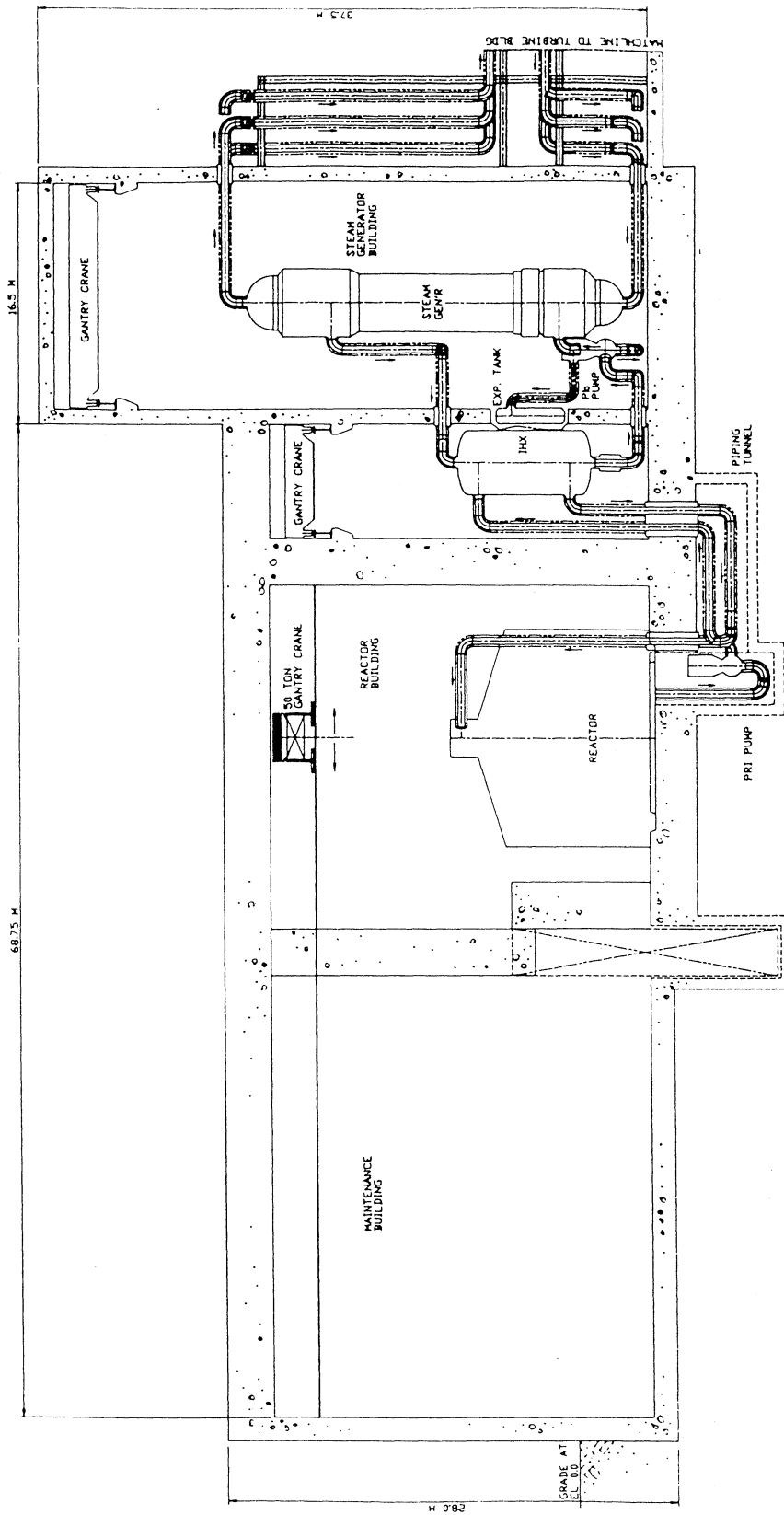


Fig. 2.3. Elevation view of Osiris reactor and steam generator buildings.

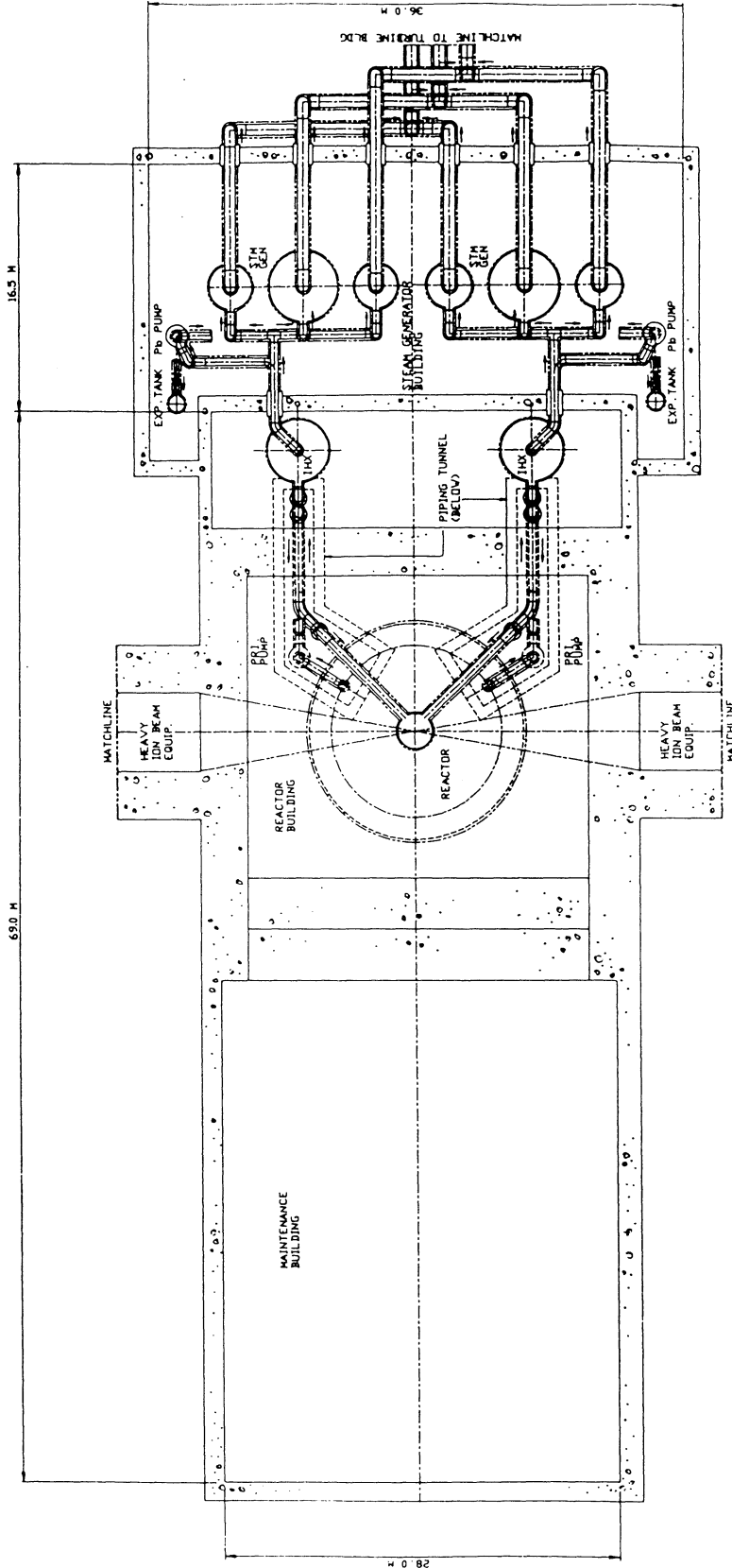


Fig. 2.4. Plan view of Osiris reactor and steam generator buildings.

We found significant cost savings by choosing our driver parameters after an extensive search of the allowed driver design parameters. Driver parameters varied in our design study were

- the number of beams in the driver,
- the ion mass,
- the ion charge state,
- the quadrupole focusing field strength,
- the quadrupole spacing, and
- the type of superconductor used in the quadrupole windings (Nb-Ti or Nb₃Sn).

We examined the effect of variations in each of these driver parameters on both the driver cost and projected target gain.

We have developed powerful tools for modeling a wide variety of drivers and identified several areas where these tools could be used to quantify the benefits resulting from possible design variations and more aggressive design options.

2.4.2 General Description of the Driver

The heavy-ion induction linac for use as a driver for the Osiris power plant consists of an ion injector, a multiple beam induction accelerator to produce high beam energies and currents, a drift compression region for shortening the ion bunch lengths, and a final focusing system for reducing the beam radii to the small spot size required for target ignition.

The injector consists of a source of charged ions and a voltage gradient to accelerate the ions. The injector is followed by an injection matching section where the ion beam parameters are adjusted to match those of the accelerator focusing lattice. There are several types of sources and injectors. A simple injector could consist of a plasma-discharge ion source followed by a voltage grid. In this design, ions would be created from a gas or vapor by a discharge voltage and then accelerated between electrical voltage grids. The shape of the grids (anodes and cathodes) is designed to produce a source of ions with minimal angular divergence. We have not created a detailed design of the injector, but we have used common limits to scale the achievable injection currents with ion mass, ion charge state, and acceleration gap voltage.

The accelerator consists of a lattice of quadrupole arrays with induction cells located between the arrays. The quadrupole arrays contain a superconducting quadrupole winding around each beam tube. The quadrupole fields of adjacent quadrupoles are offset by a 90° rotation to provide an alternating focusing lattice (which is described as a focusing-drift-defocusing-drift, or FODO, lattice). Each pair of quadrupoles in a repeating FODO lattice focuses the beam in two dimensions. Inductor cells are placed between quadrupoles as shown in Fig. 2.5. Each induction cell consists of a ferromagnetic core surrounding all of the beams as shown schematically in Fig. 2.6; the cores accelerate the beams through transformer action.

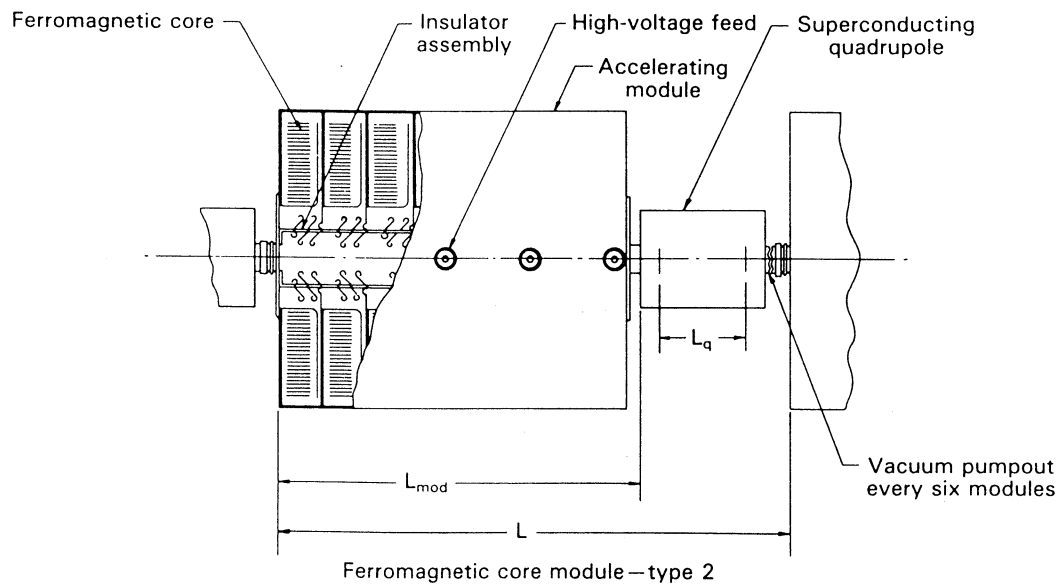


Fig. 2.5. Acceleration and focusing components in each half-lattice period.⁶

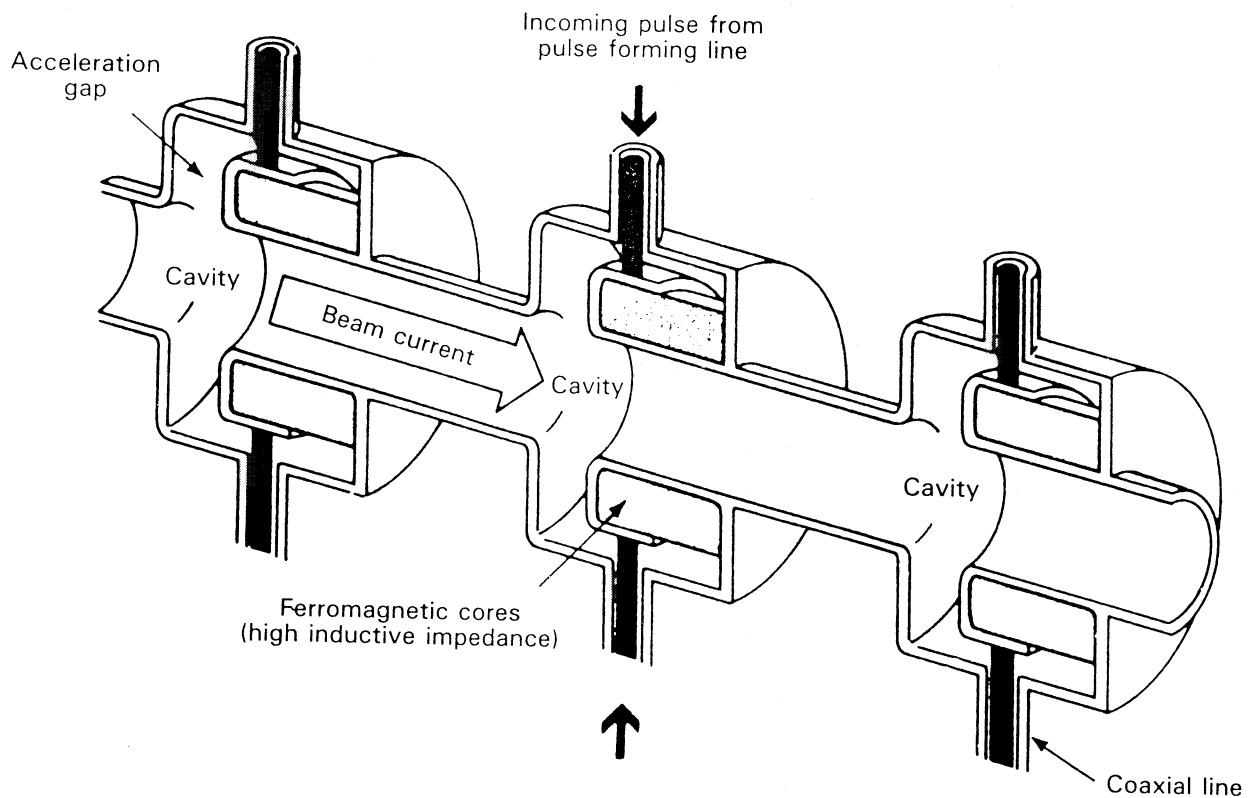


Fig. 2.6. Schematic cutaway of an induction linac.⁷

Because of the need for very short pulse durations at the target, the axial length of the pulse that comes out of the accelerator is shortened in a drift compression stage. The acceleration cells preceding the drift compression stage use shaped pulses to create a velocity tilt between the ions at the beginning and end of the pulse; this velocity tilt compresses the beam length until the velocity tilt is canceled by space-charge effects just before the beam reaches the target.

The final focusing system consists of quadrupole pairs or triplets which compress the beams to the final spot size. In order to attain the smallest possible spot sizes, the beams are spread and expanded before final focusing. The beams are also neutralized with co-injected electrons just after leaving the final focusing magnets in order to minimize space-charge effects during focusing.

Our design strategy builds upon one described by Monsler in 1987.⁸ The chosen high-energy propagation mode uses a constant effective focusing length for each quadrupole and a constant beam radius. This allows for a single quadrupole array design to be used for the entire length of the driver. The spacing of the quadrupole arrays (the linear quad packing fraction) is varied so that the beam carries the maximum allowable current at every point in the driver.

Two types of inductor cells are used. A large radial build is used in the beginning of the driver where cores and quad arrays are packed closely together, and a smaller radial build is used in the high-energy section of the driver where there are greater separations between quad arrays. The use of inductors with a smaller radial build in the longest section of the driver lowers the total required volume of core material (Metglas).

The use of a single design for the quad arrays and only two designs for the inductors simplifies manufacturing requirements and allows for maximum economy of scale for producing driver components.

Our reference design is conservative in several respects. More aggressive driver designs use beam combination, beam separation, and/or recirculation to lower driver costs. All three modifications add performance uncertainties and design complexity, so we have chosen not to use these options in our base driver. We also chose a base design using singly charged, $q = 1$, ions. Higher charge states require more complicated sources and injectors, and highly charged ions may require better vacuums because of the increased potential for beam-gas charge exchange.

2.4.3 Accelerator Design

The base design for a 5 MJ accelerator was chosen after several parametric variation studies. The optimum value for each driver parameter depends on the chosen value of all the other variables, so an iterative approach was used to set the base parameters. The chosen driver parameters led to a 4.8 km long driver shown in Fig. 2.7. The driver parameters for this base design are shown Table 2.3.

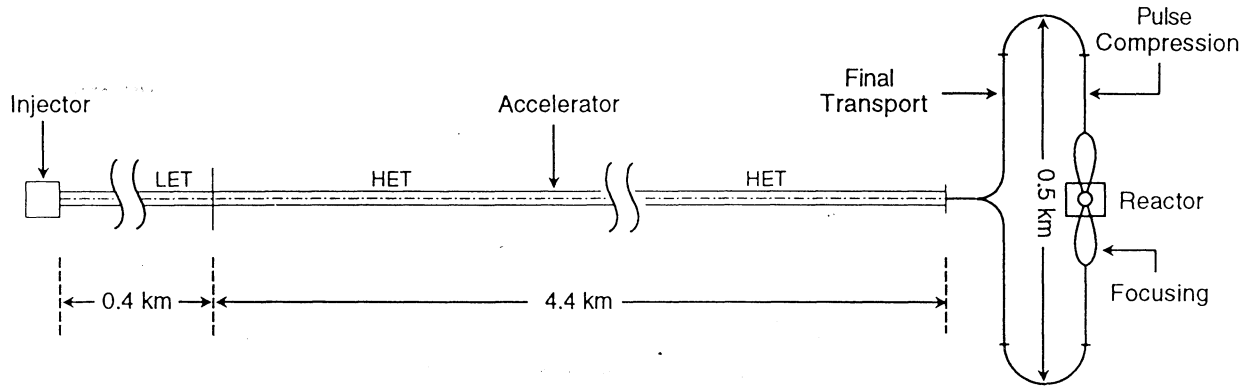


Fig. 2.7. Base heavy-ion driver schematic.

Table 2.3. Reference Parameters for HIB Driver Design

| | | | |
|-----------------------|--------------------|-------------------------------|--------|
| Energy (MJ) | 5 | Final Focus Half-angle (mrad) | 33 |
| Ion Mass (amu) | 131 | Spot Radius (mm) | 2.3 |
| Charge State | 1 | Ion Range (g/cm^2) | 0.07 |
| Superconductor | Nb ₃ Sn | Quads | |
| Number of Beams | 12 | Max. Axial Quad. Occupancy | 0.8 |
| B-max at S/C (T) | 10 | Number of Arrays | 1978 |
| Driver Efficiency (%) | 28.2 | Number of Quads | 23,736 |
| Beam Voltage | | Effective Field Length (cm) | 18.1 |
| Initial (MV) | 3 | Quad Length (cm) | 22.6 |
| Final (GV) | 3.83 | Beam Radius (cm) | 6.8 |
| Current per Beam | | Quad Bore (cm) | 8.9 |
| Initial (A) | 3.5 | LET Cores | |
| Final (kA) | 1.09 | Number | 804 |
| Pulse Length | | Length (cm) | 20 |
| Initial (ms) | 34 | Radial Build (cm) | 80 |
| Final (ns) | 100 | HET Cores | |
| Accelerator Length | | Number | 6840 |
| Low Energy (m) | 359 | Length (cm) | 10 |
| Pulse Matching (m) | 33 | Radial Build (cm) | 40 |
| High Energy (km) | 4.4 | Total Metglass (MT) | 14.3 |
| Total Length (km) | 4.8 | | |

2.4.4 Final Transport Design

The final compression and focus segment matches the 3.83 GeV Xe⁺¹ linac output beam to the parameters specified at the target. Figure 2.8 shows the layout of the final compression and focus. There is a series of three functional sections: a transport section, a compression section, and a transverse focus section. The design illustrated in Fig. 2.8 allows the use of a conservative value (51.6 m) for the average bending radius. Also, the chosen layout eliminates the problem of dispersion in the bends due to the large coherent velocity tilt of the compression phase. Overall design parameters for final compression and focus are listed in Table 2.4. Each of the three functional sections of the final transport systems is described in the following paragraphs.

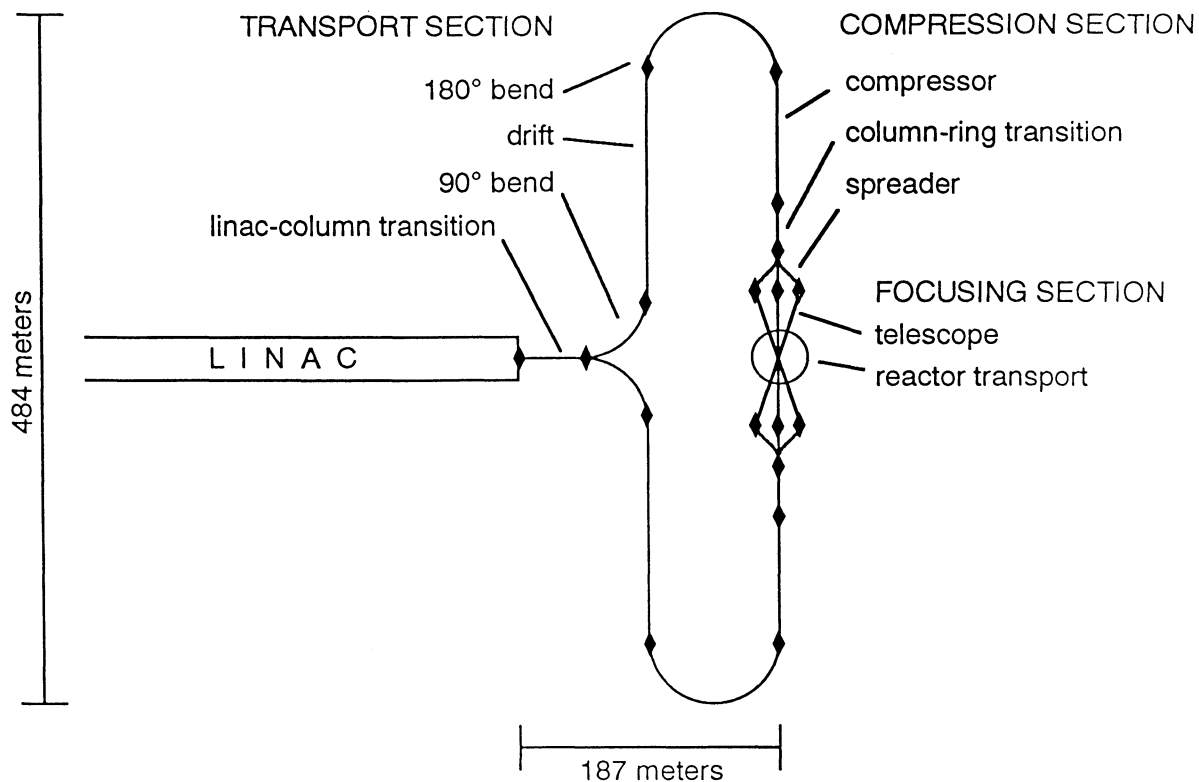


Fig. 2.8. Final compression and focus layout.

Table 2.4. Final Compression and Focus Design Parameters

| Parameter | Value |
|-------------------------------------|--------------|
| Transport Length (m) | 611 |
| Linac-to-Target Distance (m) | 187 |
| Total Width (\perp to linac) (m) | 484 |
| Number of Quadrupoles | 984 |
| Number of Dipoles | 528 |

Transport Section. The transport section splits the 12-beam bundle from the linac into two 6-beam bundles, then transports each of the 6-beam bundles so that they are aimed at the target from a sufficient distance to accommodate compression and transverse focus. The transport section is composed of four elements: an initial transition element to transform the 12-beam bundle into two 6-beam columns, a 90 degree bend to direct the columns away from the linac axis, a straight section to carry the columns the required distance from the axis, and a 180 degree bend to direct the bundles back towards the target.

Compression Section. The compression section provides the specified 10 ns longitudinal focus in the middle of the final focusing quadrupole set. The compression section is comprised of three elements: the compressor element to provide the required velocity tilt, a transition element to transform the 6-beam column into a hexagonal ring, and a spreading element to provide sufficient clearance between the beams so that the final focusing quads of adjacent beams can be packaged.

Pulse shaping to provide a pre-pulse at the target would be done by tailoring the applied voltage gradient waveform in the compressor. This approach allows an arbitrary fraction of the pulse energy to be in the pre-pulse while preserving the equivalence of the individual beams.

Transverse Focus Section. The transverse focus section delivers the longitudinally-compressed beam to the target. It consists of two elements: a focusing telescope, which provides the required convergent angle to the beam bunches, and a reactor transport element, which provides the final beam steering and the auto-neutralizing electrons immediately before the beam bunches enter the reactor chamber. Some combination of shielding, baffles, and shutters at the reactor interface must be included to protect the final focusing components from target radiation, target debris, and hot molten Flibe.